Deformations of General Parametric Shells: Computation and Robot Experiment

Yan-Bin Jia and Jiang Tian

Abstract— **A shell is a body enclosed between two closely spaced and curved surfaces. Classical theory of shells [38], [33], [16] assumes a parametrization along the lines of principal curvature on the middle surface of a shell. Such a parametrization, while always existing locally, is not known for many surfaces, and deriving one can be very difficult if not impossible. This paper generalizes the classical strain-displacement equations and strain energy formula to a shell with an arbitrary parametric middle surface. We show that extensional and shearing strains can all be represented in terms of geometric invariants including principal curvatures, principal vectors, and the related directional and covariant derivatives. Computation of strains and strain energy is also described for a general parametrization.**

The displacement field on a shell is represented as a B-spline surface. By minimization of potential energy, we have simulated deformations of algebraic surfaces under applied loads, and performed experiments on an aluminum soda can and a stretched cloth using a three-fingered Barrett Hand. The measured deformations on each object match those in the simulation with good accuracy. The presented work is an initial step in our research on robot grasping of deformable objects.

I. INTRODUCTION

Deformable objects are ubiquitous in our daily life. The ability to manipulate them is an important measure of the robot's intelligence and dexterity. Such skill expects to not only exert impact on medical robotics but also open the door for the development of home robots. Despite the rich literature on robot grasping [4] and dexterity [29], manipulation of deformable objects has remained an underdeveloped research area. This is in part due to the lack of a geometric framework to characterize this type of manipulation, and in part due to the high computational cost of modeling the physic process itself.

There are two methods of dealing with deformability in solid mechanics: the energy model based on Castigliano's theorem [11, p. 375] and the dynamic model described by Navier's equations [14, pp. 203-205]. Both methods are based on the strain-displacement relations (i.e., kinematics) and the strain-stress relations (Hooke's law). Castigliano's theorem views deformation as energy minimization. Assuming linear elasticity of isotropic and homogeneous material, the theorem states that the partial derivatives of the total strain energy with respect to a generalized displacement (force, respectively) is the corresponding generalized force (displacement, respectively). Navier's equations generate a dynamic deformable model describing shape evolution over time, which is valuable for analysis and interaction.

Department of Computer Science, Iowa State University, Ames, IA 50011, USA. `jia, jiangt@cs.iastate.edu`.

A shell is a thin body enclosed between two closely spaced and curved surfaces. In this paper, we will apply the energy method to compute the deformed shape of a parametrized shell under the contact force exerted by a robot finger. The strain energy of a linear object can be described using the tangent, curvature, and torsion functions along the shape [10, pp. 425,447;373,383]. With constraints at the endpoints, the shape of such an object can be solved for minimum potential energy by the technique of calculus of variations, or more often, by the Ritz's method which uses a linear combination of basis functions [18], [31].

Deformations of 2-$\frac{1}{2}$D objects, in particular, shells and plates, have been studied based on the geometry of their middle surfaces [38], [16], [33]. To our knowledge, all the treatments from the mechanics of materials have assumed the middle surface of a shell to be parametrized along the lines of curvature. The expressions of extensional and shear strains, and strain energy, though derived in a local frame at every point, are still dependent on the specific parametrization rather than on geometric properties only. More specifically, the parametrization dependent features in the formulation include the magnitudes of the two partial derivatives of the surface function and the change rates of these magnitudes.

Most surfaces (including the Bézier and B-spline surfaces, and NURBS used in geometric modeling) are not parametrized along the lines of curvatures. Transformation into such a parametrization can be very difficult if not impossible. This fact has prevented direct application of the strain energy form to computing deformations of general parametric surfaces.

In Section III, we will establish that the strains and strain energy of a shell under a displacement field are decided by geometric invariants including the two principal curvatures and two principal vectors. Section IV and the Appendix will outline the strain energy computation for a general parametric shell. Using a B-spline representation of the displacement field, Section V will solve for shell deformations under an applied load via energy minimization. Section VI presents simulation results on four algebraic surfaces. Experiments on a deformed soda can and a framed cloth screen are conducted in Section VII.

II. RELATED WORK

Based on Castigliano's theorem, the Finite Element Method (FEM) [35], [3] can determine the stress, strain, and displacement everywhere inside a body represented as a mesh structure. FEMs are used to model the deformations of a wide range of shapes: fabric [8], a human hand interacting

with a deformable object [17], human tissue deformation in a surgery [5], etc. An FEM [7] is described for the analysis of thin shells based on the Kirchhoff-Love theory and smooth interpolation of displacement fields. Subdivision surfaces are used and results are shown for planar, cylindrical, and spherical shells only.

However, FEMs require extensive computation and often have to be simulated off-line, and do not work well on modeling large deformations. The boundary element method (BEM) [19] solves for boundary displacement and forces through a conversion of Navier's equations to one defined on the shape boundary. It is more efficient and accurate for computing contact force. The skeleton-based method [22] achieves efficiency of deformable modeling by computing the stresses/strains at contact points and geometrically salient points and then by interpolating over the entire surface.

Work on robotic manipulation of deformable objects has been mostly limited to linear and meshed objects [41], [26]. Most of the developed models are energy-based and some are not experimentally verified. Picking up a highly flexible linear object such as a wire or rope can be easily done with a vision system [32]. Knotting [34], [24], unknotting [20], and both [40] are the typical manipulation operations on this type of linear objects.

In graphics, the primary focus of deformable modeling is on efficient computation of effects that look like real, rather than on accurate modeling of the physical world. Discrepancies with the theory of elasticity are tolerated, and experiments with real objects need not be conducted. For instance, the widely used formulation [36] on surface strain energy[1] does not follow from solid mechanics. In this field, there are generally two approaches of modeling deformable objects: geometry-based and physics-based [15]. In a geometry-based approach, splines and spline surfaces such as Bézier curves, B-splines, non-uniform rational B-splines (NURBS), are often used as representations [2], [12].

Physics-based modeling [27] of deformation takes into account the mechanics of materials and dynamics to a certain degree. Mass-spring systems, though inaccurate and slow for simulating material with high stiffness, are used extensively in animation [6], facial modeling [42], [37], and simulations of cloth [1], animals [39], and surgery [9]. The "snake model", meanwhile, is widely used in medical image analysis [25].

III. SHELL DEFORMATIONS

Throughout the paper, we adopt the notation f_u for the partial derivative of a function $f(u, v)$ with respect to u.

A. Some Background in Surface Geometry

Let $\boldsymbol{\sigma}(u, v)$ be a surface patch in 3D such that the tangent plane at every point p is spanned by the two partial derivatives $\boldsymbol{\sigma}_u$ and $\boldsymbol{\sigma}_v$ with respect to u and v, respectively. The unit normal to the surface is $\boldsymbol{n} = \boldsymbol{\sigma}_u \times \boldsymbol{\sigma}_v / \|\boldsymbol{\sigma}_u \times \boldsymbol{\sigma}_v\|$.

[1] defined to be the integral sum of the squares of the norms of the changes in the first and second fundamental forms.

The *first fundamental form* of $\boldsymbol{\sigma}$ is defined as $E du^2 + 2F du dv + G dv^2$, where

$$E = \boldsymbol{\sigma}_u \cdot \boldsymbol{\sigma}_u, \quad F = \boldsymbol{\sigma}_u \cdot \boldsymbol{\sigma}_v, \quad G = \boldsymbol{\sigma}_v \cdot \boldsymbol{\sigma}_v; \quad (1)$$

and the *second fundamental form* as $L du^2 + 2M du dv + N dv^2$, where

$$L = \boldsymbol{\sigma}_{uu} \cdot \boldsymbol{n}, \quad M = \boldsymbol{\sigma}_{uv} \cdot \boldsymbol{n}, \quad N = \boldsymbol{\sigma}_{vv} \cdot \boldsymbol{n}. \quad (2)$$

A compact representation of the two fundamental forms use the following two symmetric matrices:

$$\mathcal{F}_I = \begin{pmatrix} E & F \\ F & G \end{pmatrix} \quad \text{and} \quad \mathcal{F}_{II} = \begin{pmatrix} L & M \\ M & N \end{pmatrix}. \quad (3)$$

The two *principal curvatures* κ_1 and κ_2 at a point p are the eigenvalues of $\mathcal{F}_I^{-1} \mathcal{F}_{II}$. They represent the maximum and minimum rates of the change of geometry when passing through p at unit speed on the patch, and are achieved in two orthogonal velocity directions, respectively, unless $\kappa_1 = \kappa_2$. These two directions, represented by unit vectors $\boldsymbol{t}_1$ and $\boldsymbol{t}_2$, are referred to as the *principal vectors*. The two principal vectors and the unit normal $\boldsymbol{n} = \boldsymbol{t}_1 \times \boldsymbol{t}_2$ define the *Darboux frame* at the point.

The patch is *orthogonal* if $F = 0$ everywhere. It is *principal* if $F = M = 0$ everywhere. On a principal patch, the principal curvatures are simply $\kappa_1 = L/E$ and $\kappa_2 = N/G$, respectively, and the corresponding principal vectors are $\boldsymbol{t}_1 = \boldsymbol{\sigma}_u / \sqrt{E}$ and $\boldsymbol{t}_2 = \boldsymbol{\sigma}_v / \sqrt{G}$.

B. Middle Surface as a Principal Patch

This section reviews some known results on deformations and strain energy from the theory of shells in solid mechanics, which, to our knowledge, have treated principal patches only. In Section III-C, we will transform these results to make them independent of a specific parametrization. but rather dependent on geometric invariants including principal curvatures and vectors.

Our treatment is from [16] with some changes of notation. We look at a section of the shell and let its middle surface before deformation be described by a principal patch $\boldsymbol{\sigma}(u, v)$, as shown in Fig. 1(a). Every point p in the shell is along the normal direction of some point $q = \boldsymbol{\sigma}(u, v)$ on the middle surface (see Fig. 1(b)). In other words, q is the projection of p onto $\boldsymbol{\sigma}$.

The displacement $\boldsymbol{\delta}(u, v)$ of q is best described in its Darboux frame:

$$\boldsymbol{\delta}(u, v) = \alpha(u, v)\boldsymbol{t}_1 + \beta(u, v)\boldsymbol{t}_2 + \gamma(u, v)\boldsymbol{n}.$$

We refer to the vector field $\boldsymbol{\delta}(u, v)$ as the *displacement field* of the shell, which yields the new position q' of q:

$$q' = \boldsymbol{\sigma}'(u, v) = \boldsymbol{\sigma}(u, v) + \boldsymbol{\delta}(u, v).$$

The new position p' of the point p may not be along the normal direction of q', due to a *transverse shear strain* that acts on the surface through p and parallel to the middle surface. This type of strain tends to be much smaller than other types of strains on a shell and is neglected by classical
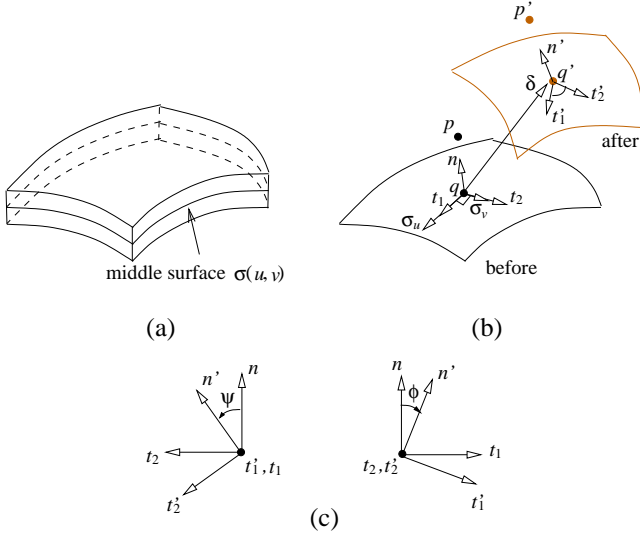
Fig. 1. Deformation of a shell: (a) before; (b) points p and q and their displace locations p' and q'; (c) rotation of the surface normal.

solution techniques like [21], [38]. It is also not considered in this paper.

At q there are *extensional strains* ε_1 and ε_2, which are the relative increases in lengths along the two principal directions t_1 and t_2, respectively. There is also the *in-plane shear strain* ω defined as the change of the angle between t_1 and t_2 under deformation. As shown in Fig. 1(b), t'_1 and t'_2 are the unit tangents along the two partial derivatives of σ', respectively. The angle between t'_1 and t'_2 is no longer $\pi/2$, and ω is the negative change. We have from [16, p. 219]:

$$\varepsilon_1 = \frac{\alpha_u}{\sqrt{E}} + \frac{(\sqrt{E})_v}{\sqrt{EG}} \cdot \beta - \kappa_1 \gamma, \tag{4}$$

$$\varepsilon_2 = \frac{\beta_v}{\sqrt{G}} + \frac{(\sqrt{G})_u}{\sqrt{EG}} \cdot \alpha - \kappa_2 \gamma, \tag{5}$$

$$\omega = \frac{\beta_u}{\sqrt{E}} - \frac{(\sqrt{E})_v}{\sqrt{EG}} \cdot \alpha - \frac{(\sqrt{G})_u}{\sqrt{EG}} \cdot \beta + \frac{\alpha_v}{\sqrt{G}}, \tag{6}$$

The extensional and in-plane shear strains at p will also include some components due to the rotation of the normal n (see Figure 1(c)). Under the assumption of small deformation, we align t_1 with t'_1 and view along them. Let ψ be the amount of rotation of the normal n about the t_1 axis toward t_2. Similarly, let ϕ be the amount of rotation of the normal about the t_2 axis toward t_1. We have [16, pp.209–213]

$$\phi = -\frac{\gamma_u}{\sqrt{E}} - \alpha \kappa_1, \tag{7}$$

$$\psi = -\frac{\gamma_v}{\sqrt{G}} - \beta \kappa_2. \tag{8}$$

Let z be the (signed) distance from the middle surface to p (along the normal n). It is shown that[2] the extensional strains at p are $\varepsilon_1 + z\zeta_1$ and $\varepsilon_2 + z\zeta_2$, and the shearing strain

[2] by dropping all terms of order $h\kappa_1$ or $h\kappa_2$ when compared to 1.

is $\omega + z\tau$, where, from [16, p. 219],

$$\zeta_1 = \frac{\phi_u}{\sqrt{E}} + \frac{(\sqrt{E})_v}{\sqrt{EG}} \cdot \psi, \tag{9}$$

$$\zeta_2 = \frac{\psi_v}{\sqrt{G}} + \frac{(\sqrt{G})_u}{\sqrt{EG}} \cdot \phi, \tag{10}$$

$$\tau = \frac{\phi_v}{\sqrt{G}} - \frac{(\sqrt{G})_u}{\sqrt{EG}} \cdot \psi + \frac{\psi_u}{\sqrt{E}} - \frac{(\sqrt{E})_v}{\sqrt{EG}} \cdot \phi. \tag{11}$$

The geometric meanings of these terms will be revealed in Section III-C.

Let e be the modulus of elasticity and μ the Poisson's constant of the shell material. The strain energy of the shell with middle surface S and thickness h, after the integration of z over $[-\frac{h}{2}, \frac{h}{2}]$, is modified over [16, p. 274][3]:

$$U_\varepsilon = \frac{e}{2(1-\mu^2)} \int_S \left\{ h \left(\varepsilon_1^2 + \varepsilon_2^2 + 2\mu\varepsilon_1\varepsilon_2 + \frac{1-\mu}{2}\omega^2 \right) \right.$$
$$\left. + \frac{h^3}{12} \left(\zeta_1^2 + \zeta_2^2 + 2\mu\zeta_1\zeta_2 + \frac{1-\mu}{2}\tau^2 \right) \right\} \sqrt{EG} \, dudv. \tag{12}$$

The linear term in h is due to extension and shear, the cubic term due to bending and torsion.

C. Deformations of a General Patch

The energy formulation (12) is applicable to a surface consisting of principal patches only. Though in theory there exists a principal patch surrounding every point with unequal principal curvatures, most surfaces (except planes, cylinders, spheres, etc.) do not assume such parameterizations. Classical deformation results presented in Section III-B need to be generalized to arbitrary parametric surfaces to widen their applications.

The first step in the generalization is to rewrite the strains (4)–(11) in terms of geometric invariants such as principal curvatures and vectors that are independent of a specific parametrization. These forms are currently for a principal patch whose partial derivatives are not unit vectors (neither $E = 1$ nor $G = 1$ must hold).

Let us start with the extensional strain (4). We have that

$$\alpha_u = \lim_{\Delta u \to 0} \frac{\alpha(\sigma(u + \Delta u, v)) - \alpha(\sigma(u, v))}{\Delta u}$$
$$= \lim_{\Delta u \to 0} \frac{\alpha(\sigma(u, v) + \sigma_u \cdot \Delta u) - \alpha(\sigma(u, v))}{\Delta u}$$
$$\stackrel{\text{def}}{=} \sigma_u[\alpha]. \tag{13}$$

Here $\sigma_u[\alpha]$ is defined to be the directional derivative of α with respect to σ_u. By the linearity of the directional derivative operator, we rewrite the first summand in (4)

$$\frac{\alpha_u}{\sqrt{E}} = \frac{\sigma_u}{\sqrt{E}}[\alpha] = t_1[\alpha]. \tag{14}$$

To examine the second summand in (4), we make use of the following identity

$$(t_2)_u = \frac{(\sqrt{E})_v}{\sqrt{G}} t_1, \tag{15}$$

[3] The original energy formulation in [16] erroneously includes a quadratic term in h^2, which would result from integrating z over $[-\frac{h}{2}, \frac{h}{2}]$, which would be zero. The disappearance of the linear term is also mentioned in [28, p. 45].

which can be derived through differentiating the equations $t_1 \cdot t_2 = 0$ and $\boldsymbol{\sigma}_u \cdot \boldsymbol{\sigma}_v = 0$ with respect to α. From identity (15) we have

$$
\begin{aligned}
\frac{(t_2)_u}{\sqrt{E}} &= \lim_{\Delta u \to 0} \frac{t_2(p + \boldsymbol{\sigma}_u \cdot \Delta u) - t_2(p)}{\Delta u} \cdot \frac{1}{\sqrt{E}} \\
&= \lim_{\Delta u \sqrt{E} \to 0} \frac{t_2\left(p + (\boldsymbol{\sigma}_u/\sqrt{E}) \cdot \Delta u \sqrt{E}\right) - t_2(p)}{\Delta u \sqrt{E}} \\
&= \lim_{\Delta u \to 0} \frac{t_2(p + t_1 \cdot \Delta u) - t_2(p)}{\Delta u} \\
&\stackrel{\text{def}}{=} \nabla_{t_1} t_2.
\end{aligned}
\tag{16}
$$

The *covariant derivative* $\nabla_{t_1} t_2$ measures the initial rate of change of the principal vector t_2 as the point p moves in the t_1 direction at unit speed. Combine equations (15) and (16):

$$
\begin{aligned}
\frac{(\sqrt{E})_v}{\sqrt{EG}} t_1 &= \nabla_{t_1} t_2, \quad \text{and hence} \\
\frac{(\sqrt{E})_v}{\sqrt{EG}} &= \nabla_{t_1} t_2 \cdot t_1.
\end{aligned}
\tag{17}
$$

Substitutions of equations (14) and (17) into (4) gives a formulation of the extensional strain ε_1 independent of parametrization:

$$
\begin{aligned}
\varepsilon_1 &= t_1[\alpha] + (\nabla_{t_1} t_2 \cdot t_1)\beta - \kappa_1 \gamma \\
&= t_1[\alpha] + (\nabla_{t_1} t_2 \cdot t_1)\beta + (\nabla_{t_1} n \cdot t_1)\gamma.
\end{aligned}
\tag{18}
$$

The last step uses an equivalent definition: $\kappa_i \stackrel{\text{def}}{=} -\nabla_{t_i} n \cdot t_i$. From (18) the extensional strain in a principal direction consists of three components: the change rate of the displacement in that direction, and the shearing effects caused by the displacements along the other two orthogonal directions.

Similarly, parametrization independent formulations can be derived for strain components (5)–(11):

$$
\begin{aligned}
\varepsilon_2 &= t_2[\beta] + (\nabla_{t_2} t_1 \cdot t_2)\alpha + (\nabla_{t_2} n \cdot t_2)\gamma, &\quad (19) \\
\omega &= t_1[\beta] - (\nabla_{t_1} t_2 \cdot t_1)\alpha + t_2[\alpha] - (\nabla_{t_2} t_1 \cdot t_2)\beta, &\quad (20) \\
\phi &= -t_1[\gamma] + (\nabla_{t_1} n \cdot t_1)\alpha, &\quad (21) \\
\psi &= -t_2[\gamma] + (\nabla_{t_2} n \cdot t_2)\beta, &\quad (22) \\
\zeta_1 &= t_1[\phi] + (\nabla_{t_1} t_2 \cdot t_1)\psi, &\quad (23) \\
\zeta_2 &= t_2[\psi] + (\nabla_{t_2} t_1 \cdot t_2)\phi, &\quad (24) \\
\tau &= t_1[\psi] - (\nabla_{t_1} t_2 \cdot t_1)\phi + t_2[\phi] - (\nabla_{t_2} t_1 \cdot t_2)\psi. &\quad (25)
\end{aligned}
$$

The angles ϕ and ψ represent the rotations of the normal about the two principal directions as a result of the deformation.

The geometric meanings of ζ_1, ζ_2, and τ now become clear. The term ζ_1 (ζ_2, respectively), referred to as *change in curvature*, accounts for the change rate of the angle ϕ (ψ, resp.) along the principal direction t_1 (t_2, resp.), plus the effect of the angle ψ (ϕ, resp.) due to the change of t_2 (t_1, resp.) along t_1 (t_2, resp.). Together, ζ_1 and ζ_2 measure the bending of the surfaces. The term τ, referred to as *change in torsion*, measures the twising of the surface due to the deformation.

In the energy integral (12), the area element $\sqrt{EG}\,dudv$ now needs to be replaced by $\sqrt{EG - F^2}\,dudv$ since $\boldsymbol{\sigma}_u$ and $\boldsymbol{\sigma}_v$ are no longer necessarily orthogonal.

Theorem 1: The strain energy of a shell under a displacement field depends on the principal curvatures and the principal directions of its middle surface. More specifically, it is the integral (12) with $\sqrt{EG}\,dudv$ replaced by $\sqrt{EG - F^2}\,dudv$ and all strains given in (18)–(25).

IV. A Patch with General Parametrization

To obtain the strains according to equations (18)–(25), we need to be able to compute the directional derivatives of the principal curvatures κ_1, κ_2 and the displacements α, β, γ with respect to the principal vectors t_1 and t_2, as well as the covariant derivatives $\nabla_{t_i} t_j$, $i, j = 1, 2$ and $i \neq j$. All these derivatives should be expressed in terms of the parameters u and v.

A. Differentiation of Principal Curvatures

The *Gaussian* and *mean curvatures* are respectively the determinant and half the trace of the matrix $\mathcal{F}_I^{-1} \mathcal{F}_{II}$:

$$
\begin{aligned}
K &= \kappa_1 \cdot \kappa_2 = \frac{LN - M^2}{EG - F^2}, &\quad (26) \\
H &= \frac{\kappa_1 + \kappa_2}{2} = \frac{1}{2} \cdot \frac{EN - 2FM + GL}{EG - F^2}. &\quad (27)
\end{aligned}
$$

The principal curvatures can thus be expressed in terms of the Gaussian and mean curvatures (choosing $\kappa_1 \geq \kappa_2$) :

$$
\begin{aligned}
\kappa_1 &= H + \sqrt{H^2 - K}, &\quad (28) \\
\kappa_2 &= H - \sqrt{H^2 - K}. &\quad (29)
\end{aligned}
$$

To obtain the partial derivatives of κ_1 and κ_2 with respect to u and v, we first differentiate the fundamental form coefficients E, F, G, L, M, N defined in (1) and (2). The partial derivatives of K and H are then computed using (26) and (27). Finally, we differentiate the equations (28) and (29).

B. Covariant Derivatives of Principal Vectors

The principal vectors are linear combinations of $\boldsymbol{\sigma}_u$ and $\boldsymbol{\sigma}_v$ which span the tangent plane at p:

$$
\begin{aligned}
t_1 &= \xi_1 \boldsymbol{\sigma}_u + \eta_1 \boldsymbol{\sigma}_v, &\quad (30) \\
t_2 &= \xi_2 \boldsymbol{\sigma}_u + \eta_2 \boldsymbol{\sigma}_v. &\quad (31)
\end{aligned}
$$

Here $(\xi_1, \eta_1)^T$ and $(\xi_2, \eta_2)^T$ are the eigenvectors of $\mathcal{F}_I^{-1} \mathcal{F}_{II}$ corresponding to κ_1 and κ_2, respectively [30, p. 133]. Namely, for $i = 1, 2$, we have

$$
(\mathcal{F}_{II} - \kappa_i \mathcal{F}_I) \binom{\xi_i}{\eta_i} = 0.
\tag{32}
$$

The four coefficients ξ_i, η_i will be derived in the Appendix.

Using (30)-(31), all the derivatives with respect to the principal vectors t_1, t_2 in equations (18)–(25), repetitive or not, can now be obtained. For instance,

$$
\begin{aligned}
t_1[\alpha] &= (\xi_1 \boldsymbol{\sigma}_u + \eta_1 \boldsymbol{\sigma}_v)[\alpha] \\
&= \xi_1 \cdot \boldsymbol{\sigma}_u[\alpha] + \eta_1 \cdot \boldsymbol{\sigma}_v[\alpha] \\
&= \xi_1 \alpha_u + \eta_1 \alpha_v \qquad \text{by (13)}.
\end{aligned}
$$

We also have, for $i, j = 1, 2$,

$$
\begin{aligned}
\nabla_{t_i} t_j &= \nabla_{\xi_i \sigma_u + \eta_i \sigma_v} t_j \\
&= \xi_i \nabla_{\sigma_u} t_j + \eta_i \nabla_{\sigma_v} t_j \\
&= \xi_i \nabla_{\sigma_u} (\xi_j \sigma_u + \eta_j \sigma_v) + \eta_i \nabla_{\sigma_v} (\xi_j \sigma_u + \eta_j \sigma_v) \quad (33)
\end{aligned}
$$

We work on the first summand in the last equation above:

$$
\begin{aligned}
& \xi_i \nabla_{\sigma_u} (\xi_j \sigma_u + \eta_j \sigma_v) \\
=\; & \xi_i (\sigma_u[\xi_j] \sigma_u + \xi_j \nabla_{\sigma_u} \sigma_u + \sigma_u[\eta_j] \sigma_v + \eta_j \nabla_{\sigma_u} \sigma_v) \\
=\; & \xi_i \left(\frac{\partial \xi_j}{\partial u} \sigma_u + \xi_j \sigma_{uu} + \frac{\partial \eta_j}{\partial u} \sigma_v + \eta_j \sigma_{uv} \right).
\end{aligned}
$$

The first step above uses a fact about covariant derivatives: $\nabla_a(f\boldsymbol{b}) = \boldsymbol{a}[f] \cdot \boldsymbol{b} + f \cdot \nabla_a \boldsymbol{b}$. The second step uses the fact shown in (13). Namely, the directional derivatives of a scalar along σ_u and σ_v, respectively, are just its partial derivatives with respect to u and v. The same rule applies to the covariant derivatives of a vector with respect to σ_u and σ_v. Similarly, we express the second summand in equation (33) in terms of partial derivatives with respect to u and v. Merge the resulting terms from the two summands:

$$
\begin{aligned}
\nabla_{t_i} t_j =\; & \left(\xi_i \frac{\partial \xi_j}{\partial u} + \eta_i \frac{\partial \xi_j}{\partial v} \right) \sigma_u + \left(\xi_i \frac{\partial \eta_j}{\partial u} + \eta_i \frac{\partial \eta_j}{\partial v} \right) \sigma_v \\
& + \xi_i \xi_j \sigma_{uu} + (\xi_i \eta_j + \xi_j \eta_i) \sigma_{uv} + \eta_i \eta_j \sigma_{vv}. \quad (34)
\end{aligned}
$$

V. Energy Based Solution of Displacement Field

The displacement field $\boldsymbol{\delta}(u,v) = (\alpha, \beta, \gamma)$ of the middle surface of a shell describes the deformations completely. By minimizing the total potential energy, we can obtain the displacement field and thus determine the deformed shape.

A. B-spline Based Displacement Field

The standard FEM discretizes the shell domain and approximates the displacement values via interpolation. The generated surface often has a large number of degrees of freedom (DOFs) and may become unnecessarily complicated. To reduce the number of DOFs, we use a B-spline surface to approximate the displacement field.

A B-spline curve is a linear combination of a number of control points, each scaled by a basis function $B_{i,k}(t)$. These functions are determined by a knot vector $(t_0, \cdots, t_m)$, $t_0 < t_1 < \cdots < t_m$, and constructed over polynomials of degree k. Each basis function $B_{i,k}(t)$ is defined over the interval $[t_i, t_{i+k}]$, and has local control of the B-spline: moving one control point only alters the curve locally [23, p. 182]. The values of $B_{i,k}(t)$, $i = 1, \cdots, n$, are non-negative and satisfy the property $\sum_{i=0}^{n} B_{i,k}(t) = 1$.

A B-spline surface is defined over a $(n_1 + 1) \times (n_2 + 1)$ grid of control points $\boldsymbol{p}_{i,j}$ using two B-spline curves:

$$
S(u,v) = \sum_{i=0}^{n_1} \sum_{j=0}^{n_2} \boldsymbol{p}_{i,j} B_{i,k_1}(u) \tilde{B}_{j,k_2}(v).
$$

Every basis function of the surface is a product of two basis functions, one for each B-spline curve. The properties of a B-spline surface are similar to those of a B-spline curve, which include local control and

$$
\sum_{i=0}^{n_1} \sum_{j=0}^{n_2} B_{i,k_1}(u) \tilde{B}_{j,k_2}(v) = 1. \quad (35)
$$

We represent the displacement field $\boldsymbol{\delta}(u,v)$ as a B-spline surface:

$$
\boldsymbol{\delta}(u,v) = \sum_{i=0}^{n_1} \sum_{j=0}^{n_2} \boldsymbol{\delta}_{i,j} B_{i,k_1}(u) \tilde{B}_{j,k_2}(v), \quad (36)
$$

where $\boldsymbol{\delta}_{i,j}$ is the displacement of the (i,j)-th control point in the grid domain. Property (35) ensures that the displacement field is invariant under affine transformations, and can be exactly reproduced by interpolation. For given parameter values (u,v), the displacement $\boldsymbol{\delta}(u,v)$ is only decided by $k_1 \times k_2$ nodal displacements, which ensures a sparse discretization of the displacement field.

B. Energy Minimization

Let us get back and look at the direct relationship between the elastic potential energy U_ε and the displacements. Let $\boldsymbol{\Delta}$ be the collection of $3m$ unknowns describing the displacements at the m control points, we rewrite the strain energy U_ε in Theorem 1 into a form as

$$
U_\varepsilon = \boldsymbol{\Delta}^T K_s \boldsymbol{\Delta}, \quad (37)
$$

where K_s is the (symmetric) stiffness matrix.

Let U_q be the work done by applied loads, and $\boldsymbol{q}(u,v)$ the load vector. We have

$$
U_q = \int_S \boldsymbol{q}(u,v) \cdot \boldsymbol{\delta}(u,v) \, d\mathcal{A} = \boldsymbol{\Delta}^T Q, \quad (38)
$$

where Q is the vector of all nodal forces. The total potential energy of a shell is

$$
U = U_\varepsilon - U_q = \boldsymbol{\Delta}^T K_s \boldsymbol{\Delta} - \boldsymbol{\Delta}^T Q. \quad (39)
$$

The equilibrium state of an elastic shell has minimum total potential energy [13, p. 260]. We need to *find a displacement field which minimizes U and satisfies the boundary conditions*.

The boundary constraints are formulated as an integral over the boundary curve. Let $\boldsymbol{r}(u,v)$ be the position describing the boundary Ω of the middle surface $\boldsymbol{\sigma}(u,v)$ of a shell, we minimize

$$
\int_\Omega \left(\boldsymbol{\sigma}(u,v) - \boldsymbol{r}(u,v) \right)^2 d\ell. \quad (40)
$$

At the minimum of this integral, the vanishing of its partial derivatives with respect to all nodal displacements yields a system of linear equations

$$
P\boldsymbol{\Delta} = R. \quad (41)
$$

Each equation represents a single linear constraint generated by differentiating the integral with respect to one component of $\boldsymbol{\Delta}$.

To obtain the displacement field, we need to minimize the energy function defined in (39) while satisfying the linear equations in (41), that is

$$\min \boldsymbol{\Delta}^T K_s \boldsymbol{\Delta} - \boldsymbol{\Delta}^T Q \quad \text{where} \quad P\boldsymbol{\Delta} = R.$$

By introducing a vector $\boldsymbol{\lambda}$ of Lagrange multipliers, the problem is equivalent to:

$$\min \boldsymbol{\Delta}^T K_s \boldsymbol{\Delta} - \boldsymbol{\Delta}^T Q + (P\boldsymbol{\Delta} - R)^T \boldsymbol{\lambda}.$$

Differentiating the objective function above with respect to $\boldsymbol{\Delta}$, we obtain

$$2K_s \boldsymbol{\Delta} + P^T \boldsymbol{\lambda} = Q, \tag{42}$$

So we have a system of linear equations (41) and (42) in terms of the nodal displacements and the Lagrange multipliers. They are solved efficiently by singular value decomposition (SVD).

VI. Simulation

We start with a fixed rectangular plate with thickness 1.25mm. Fig. 2 displays the plate before and after deformation. We set the values of the Young's modulus $e = 0.007$GPa and the Poisson's ratio $\mu = 0.33$. Under a point load of 11.12N perpendicular to the plate, the calculated maximum displacement is 2.39mm.
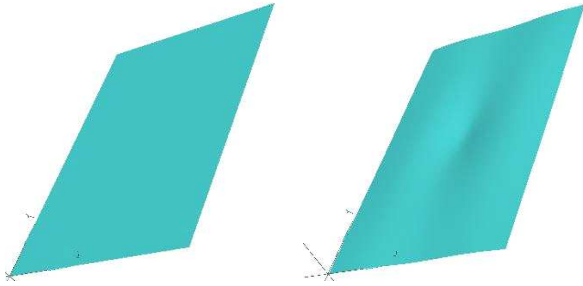
Fig. 2. A fixed plate before (left) and after (right) deformation.

Simulation tests are also conducted on three other fixed surfaces including a half cylinder, a half ellipsoid, and a monkey saddle. The results are shown in Fig. 3. Table I lists their mechanical properties, and the maximum displacements.
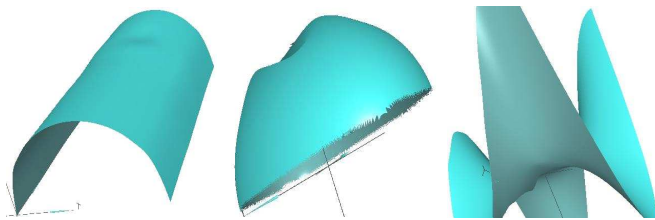
Fig. 3. Three more deformed shapes in simulation: a half cylinder, a half ellipsoid, and a monkey saddle.

object	cylinder	ellipsoid	monkey saddle
e (GPa)	0.007	0.007	0.007
μ	0.33	0.33	0.33
thickness (mm)	1.25	1.25	1.25
max disp. (mm)	2.16	13.48	8.32
point load (N)	4.0	22.24	8.9

TABLE I

MECHANICAL PROPERTIES AND MAXIMUM DISPLACEMENTS OF THE OBJECTS USED IN SIMULATION.

Fig. 4. Experimental setup with a screen and a cylinder.

VII. Experiment

The system setup is shown in Fig. 4. A three-fingered Barrett Hand is mounted on an Adept Cobra 600 robot. Every finger has a strain gauge sensor that measures contact force. A mesh model for the deformed surface due to finger contact is generated[4] by the NextEngine's desktop 3D scanner, which has an accuracy of 0.127mm. Two fixed objects with thickness 1.0mm are used in our experiments, a screen and a soda can. The values of Young's modulus e are set as 0.000007GPa and 68.9GPa, the values of Poisson's ratio μ are set as 0.3 and 0.33 for the screen and the cylinder, respectively.

We measure the accuracy by matching the computed deformed surfaces against the corresponding triangular mesh models. The visibly deformed areas have approximate sizes of 60mm × 80mm on the screen and 50mm × 80mm on the cylinder. As far as the number of control points is concerned, we create several B-spline surfaces with different numbers of control points and compare the results. We find the results are similar when there are more than 100 control points, which means that as the B-spline surface is refined, the solution converges to the real deformation result. When there are more than 100 control points, adding more control points does not increase the accuracy dramatically but increase the computational cost. The test result agrees with the standard FEM convergence property. In our experiments, we use 121 control points. The computation time is less than 10 seconds.

Table II lists, for each object, the maximum measured

[4]Due to occlusions, the deformed surface is scanned at different orientations and the resulting patches are combined.

displacement, the corresponding computed displacement, the average and the maximum errors of all points. In this table, the average errors are relatively small. Since there is no strict border between small deformations and large deformations, and the linear elastic theory is only appropriate for small deformations, the maximum errors are relatively large. We expect to decrease the maximum errors by incorporating nonlinear theory. In the experiments, we also find that the measured deformations on each object and the simulated ones are close.

	measured max disp.	computed disp.	average error	max error
screen	9.78	7.80	0.91	4.95
cylinder	1.42	1.19	0.35	1.32

TABLE II

MAXIMUM DISPLACEMENTS AND ERRORS (MILLIMETERS).

VIII. Discussion and Future work

This paper transforms the classical formulations of deformations and strain energy of a shell so that they depend only on geometric invariants including principal curvatures and directions not on a specific parametrization. It then describes a procedure that computes the strain energy of a shell whose middle surface is arbitrarily parametrized. The B-spline representation of the displacement field allows us to efficiently compute deformations on a parametric surface under applied loads through the minimization of total potential energy. Simulation results are shown on various algebraic surfaces, a couple of which are experimentally verified with a Barrett Hand for verification.

Compared with other FEM methods for classical shell theory, we do not assume the middle surface of a shell to be parametrized along lines of curvature. Therefore, our work enlarges the scope of application to include non-trivial algebraic surfaces as well as free form surfaces which can be parametrized with NURBs or triangular B-splines. To make our work to be understood as wide as possible, we carry out deductions in the elementary differential geometry way instead of tensor calculus which consists of complicated symbols.

Experiments with more complex shapes need to be carried out in order to further verify the effectiveness of this method. In a real situation, as the object deforms, the surface regions in contact with the robot finger usually grow larger, and the load distribution changes. Also, the contact force as a function of time will influence the integration of the total energy. These factors make deformation modeling more complex, which we hope to address in our future work.

One objective in the near future is to simulate deformations on curved solid objects in an interactive environment. We will also work on large deformations that require application of nonlinear theory of elasticity.

Appendix

In the appendix, we derive the four coefficients ξ_1, η_1, ξ_2, η_2 as well as their partial derivatives with respect to u and v. Since the principal curvatures κ_i, $i = 1, 2$, are eigenvalues of the matrix $\mathcal{F}_I^{-1}\mathcal{F}_{II}$, we have

$$
\begin{aligned}
0 &= \det(\mathcal{F}_{II} - \kappa_i \mathcal{F}_I) \\
&= (L - \kappa_i E) \cdot (N - \kappa_i G) - (M - \kappa_i F)^2. \quad (43)
\end{aligned}
$$

There are two cases: (a) $L - \kappa_i E = N - \kappa_i G = 0$ for some $i = 1, 2$, and (b) either $L - \kappa_i E \neq 0$ or $N - \kappa_i G \neq 0$ for both $i = 1$ and $i = 2$.

In case (a), $M - \kappa_i F = 0$. So $\mathcal{F}_{II} - \kappa_i \mathcal{F}_I = 0$, i.e.,

$$
\mathcal{F}_I^{-1}\mathcal{F}_{II} = \kappa_i I_2,
$$

where I_2 is the 2×2 identity matrix. The two eigenvalues of $\mathcal{F}^{-1}\mathcal{F}_{II}$, namely, κ_1 and κ_2, must be equal.[5] Any tangent vector is a principal vector. We let

$$
\boldsymbol{t}_1 = \frac{\boldsymbol{\sigma}_u}{\sqrt{E}}, \quad \text{with} \quad \begin{pmatrix} \xi_1 \\ \eta_1 \end{pmatrix} = \begin{pmatrix} \frac{1}{\sqrt{E}} \\ 0 \end{pmatrix} \quad \text{by (30)}.
$$

The other principal vector $\boldsymbol{t}_2 = \xi_2 \boldsymbol{\sigma}_v + \eta_2 \boldsymbol{\sigma}_v$ is orthogonal to $\boldsymbol{t}_1$. So

$$
(\xi_2 \boldsymbol{\sigma}_u + \eta_2 \boldsymbol{\sigma}_v) \cdot \boldsymbol{\sigma}_u = 0, \quad \text{i.e.,} \quad \xi_2 E + \eta_2 F = 0. \quad (44)
$$

To determine ξ_2 and η_2, we need to use one more constraint: $\boldsymbol{t}_2 \cdot \boldsymbol{t}_2 = 1$, which is rewritten as follows,

$$
E\xi_2^2 + 2F\xi_2\eta_2 + G\eta_2^2 = 1. \quad (45)
$$

Substituting (44) into (45) yields

$$
\begin{aligned}
\xi_2 &= \mp\sqrt{\frac{F^2}{E(EG - F^2)}}, \\
\eta_2 &= \pm\sqrt{\frac{E}{EG - F^2}}.
\end{aligned}
$$

In case (b), $L - \kappa_i E \neq 0$ or $N - \kappa_i G \neq 0$ for both $i = 1, 2$. Equation (32) expands into two scalar equations according to (3):

$$
\begin{aligned}
(L - \kappa_i E)\xi_i + (M - \kappa_i F)\eta_i &= 0, \quad (46) \\
(M - \kappa_i F)\xi_i + (N - \kappa_i G)\eta_i &= 0. \quad (47)
\end{aligned}
$$

Three subcases arise for each i value.

(b1) $L - \kappa_i E = 0$ but $N - \kappa_i G \neq 0$. It follows from equation (43) that $M - \kappa_i F = 0$. Thus equation (47) gives us $\eta_i = 0$. Since $\boldsymbol{t}_i \cdot \boldsymbol{t}_i = E\xi_i = 1$, we obtain $\xi_i = \pm\frac{1}{\sqrt{E}}$.

[5]The point is said to be *umbilic*.

(b2) $L - \kappa_i E \neq 0$ but $N - \kappa_i G = 0$. This is the symmetric case of (b1). The coefficients are

$$\begin{pmatrix} \xi_i \\ \eta_i \end{pmatrix} = \begin{pmatrix} 0 \\ \pm \frac{1}{\sqrt{G}} \end{pmatrix}.$$

(b3) $L - \kappa_i E \neq 0$ and $N - \kappa_i G \neq 0$. From equation (46) we have

$$\xi_i = -\frac{M - \kappa_i F}{L - \kappa_i E} \eta_i. \tag{48}$$

Substitution of the above into (45) yields a quadratic equation with the solution

$$\eta_i = \pm \sqrt{\frac{L - \kappa_i E}{EN - 2FM + LG - 2\kappa_i(EG - F^2)}}. \tag{49}$$

In all expressions of ξ_i and η_i, the signs are chosen such that $\boldsymbol{t}_1 \times \boldsymbol{t}_2 = \boldsymbol{n}$.

The gradients $\nabla \xi_i = \left(\frac{\partial \xi_i}{\partial u}, \frac{\partial \xi_i}{\partial v} \right)$ and $\nabla \eta_i = \left(\frac{\partial \eta_i}{\partial u}, \frac{\partial \eta_i}{\partial v} \right)$, $i = 1, 2$, are obtained by differentiating appropriate forms of ξ_i and η_i that hold for all points in some neighborhood (but necessarily the ones at the point).

References

[1] David Baraff and Andrew Witkin. Large steps in cloth simulation. In *Proceedings of ACM SIGGRAPH*, pages 43–54, 1998.

[2] R. Bartels, J. Beatty, and B. Barsky. *An Introduction to Splines for Use in Computer Graphics and Geometric Modeling*. Morgan Kaufmann, Los Altos, 1987.

[3] K. J. Bathe. *Finite Element Procedures*. Prentice Hall, 1996.

[4] Antonio Bicchi and Vijay Kumar. Robotic grasping and contact: a review. In *Proceedings of the IEEE International Conference on Robotics and Automation*, pages 348–353, 2000.

[5] M. Bro-Nielsen and S. Cotin. Real-time volumetric deformable models for surgery simulation using finite elements and condensatoin. In *Proceedings of Eurographics*, pages 15:57–66, 1996.

[6] J. Chadwick, D. Haumann, and R. Parent. Layered construction for deformable animated characters. In *Proceedings of ACM SIGGRAPH*, pages 243–252, 1989.

[7] Fehmi Cirak, Michael Ortiz, and Peter Schröder. Subdivision surfaces: a new paradigm for thin-shell finite-element analysis. *International Journal for Numerical Methods in Engineering*, 47(12):2039–2072, 2000.

[8] J. Collier, B. Collier, G. O'Toole, and S. Sargand. Drape prediction by means of finite-element analysis. *Journal of the Textile Institute*, 82(1):96–107, 1991.

[9] François Conti, Oussama Khatib, and Charles Baur. Interactive rendering of deformable objects based on a filling sphere modeling approach. In *Proceedings of the IEEE International Conference on Robotics and Automation*, pages 3716–3721, 2003.

[10] Stephen H. Crandall, Norman C. Dahl, and Thomas J. Lardner. *An Introduction to the Mechanics of Solids*. McGraw-Hill, Inc., 2nd edition, 1978.

[11] Martin A. Eisenberg. *Introduction to the Mechanics of Solids*. Addison-Wesley, 1980.

[12] G. Farin. *Curves and Surfaces for Computer Aided Geometric Design*. Academic Press, Inc., 2 edition, 1990.

[13] R. T. Fenner. *Engineering Elasticity: Application of Numerical and Analytical Techniques*. Ellis Horwood, Ltd., 1986.

[14] Y. C. Fung and P. Tong. *Classical and Computational Solid Mechanics*. World Scientific, 2001.

[15] Sarah F. Gibson and Brian Mirtich. A survey of deformable models in computer graphics. Technical Report TR-97-10, Mitsubishi Electric Research Laboratories, 1997.

[16] Philip L. Gould. *Analysis of Plates and Shells*. Prentice-Hall, 1999.

[17] J. P. Gourret, N. Magnenat-Thalmann, and D. Thalmann. Simulation of object and human skin deformations in a grasping task. In *Proceedings of ACM SIGGRAPH*, pages 21–30, 1989.

[18] S. Hirai. Energy-based modeling of deformable linear objects. In Dominik Henrich and Heinz Wörn, editors, *Robot Manipulation of Deformable Objects*, pages 11–27. Springer-Verlag, 2000.

[19] Doug L. James and Dinesh K. Pai. Artdefo: accurate real time deformable objects. In *Proceedings of ACM SIGGRAPH*, pages 65–72, 1999.

[20] Andrew M. Ladd and Lydia E. Kavraki. Using motion planning for knot untangling. *International Journal of Robotics Research*, 23(7):797–808, 2004.

[21] A. E. H. Love. *A Treatise on the Mathematical Theory of Elasticity*. Dover, New York, N.Y., 4 edition, 1927.

[22] Qi Luo and Jing Xiao. Contact and deformation modeling for interactive environments. *IEEE Transactions on Robotics*, 23(2):416–430, 2007.

[23] D. Marsh. *Applied Geometry for Computer Graphics and CAD*. Springer-Verlag, 1999.

[24] Takayuki Matsuno and Toshio Fukuda. Manipulation of flexible rope using topological model based on sensor information. In *Proceedings of the IEEE/RSJ International Conference on Intelligent Robots and Systems*, pages 2638–2643, 2006.

[25] Tim McInerney and Demetri Terzopoulos. Deformable models in medical image analysis: a survey. *Medical Image Analysis*, 1(2):91–108, 1996.

[26] Mark Moll and Lydia E. Kavraki. Path planning for deformable linear objects. *IEEE Transactions on Robotics and Automation*, 22(4):625–636, 2006.

[27] Andrew Nealen, Matthias Müller, Richard Keiser, Eddy Boxerman, and Mark Carlson. Physically based deformable models in computer graphics. In *Proceedings of ACM SIGGRAPH*, 2005.

[28] V. V. Novozhilov. *Thin Shell Theory*. P. Noordhoff, Ltd., 1964.

[29] A. M. Okamura, N. Smaby, and M. R. Cutkosky. An overview of dexterous manipulation. In *Proceedings of the IEEE International Conference on Robotics and Automation*, pages 255–262, 2000.

[30] Andrew Pressley. *Elementary Differential Geometry*. Springer-Verlag, 2001.

[31] A. Remde and D. Henrich. Direct and inverse simulation of deformable linear objects. In Dominik Henrich and Heinz Wörn, editors, *Robot manipulation of deformable objects*, pages 43–70. Springer-Verlag, 2000.

[32] Axel Remde, Dominik Henrich, and Heinz Worn. Picking-up deformable linear objects with industrial robots. In *Proceedings of the International Symposium on Robotics*, 1999.

[33] Adel S. Saada. *Elasticity: Theory and Applications*. Krieger Publishing Company, 1993.

[34] Mitul Saha and Pekka Isto. Motion planning for robotic manipulation of deformable linear objects. In *Proceedings of the IEEE International Conference on Robotics and Automation*, pages 2478–2484, 2006.

[35] L. Segerlind. *Applied Finite Element Analysis*. John Wiley and Sons, New York, 1984.

[36] D. Terzopoulos, J. C. Platt, and A. H. Barr. Elastically deformable models. In *Proceedings of ACM SIGGRAPH*, pages 205–214, 1987.

[37] D. Terzopoulos and K. Waters. Physically-based facial modeling, analysis, and animation. *Journal of Visualization and Computer Animation*, 1:73–80, 1990.

[38] Stephen P. Timoshenko and S. Woinowsky-Krieger. *Theory of Plates and Shells*. McGraw-Hill, 2 edition, 1959.

[39] X. Tu and D. Terzopoulos. Artificial fishes: physics, locomotion, perception, behavior. In *Proceedings of ACM SIGGRAPH*, pages 43–50, 1994.

[40] Hidefumi Wakamatsu, Eiji Arai, and Shinichi Hirai. Knotting/unknotting manipulation of deformable linear objects. *International Journal of Robotics Research*, 25(4):371–395, 2006.

[41] Hidefumi Wakamatsu and Shinichi Hirai. Static modeling of linear object deformation based on differential geometry. *International Journal of Robotics Research*, 23(3):293–311, 2004.

[42] K. Waters. A muscle model for animating three-dimensional facial expression. In *Proceedings of ACM SIGGRAPH*, pages 17–24, 1987.